Electronic Supplementary Material (ESI) for Journal of Materials Chemistry C.

SUPPORTING INFORMATION

Reversible dehydration-hydration process in stable bismuth-based hybrid perovskites

A. A. Babaryk[1$], Y. Pérez[1,2$], M. Martínez[3], M. E. G. Mosquera[4], M. H. Zehender[3], S. A. Svatek[3], E. Antolín[3], P. Horcajada[1,*]

[1] Advanced Porous Materials Unit, IMDEA Energy Institute, Avda. Ramón y Cajal 3, 28935 Móstoles-Madrid, Spain

[2] Departamento de Biología y Geología, Física y Química Inorgánica. ESCET. Universidad Rey Juan Carlos, 28933 Móstoles (Madrid)

[3] Instituto de Energía Solar, Universidad Politécnica de Madrid, Avda. Complutense 30, 28040 Madrid, Spain

[3] Departamento de Química Orgánica y Química Inorgánica, Universidad de Alcalá, Campus Universitario, 28871 Alcalá de Henares, Spain

[$] equally contributing authors

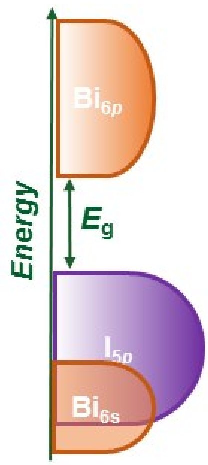

Scheme 1. General density of electronic states diagram for [BiI_4] species.

Table S1. Selective bond lengths and angles for RT and HT phases.

M-X	Bond length, [Å]	X-M-X	Bond angle, [°]
		RT-phase	
Bi1-I4	2.9092(7)	I1-Bi1-I2	171.73(2)
Bi1-I3	2.9232(7)	I1-Bi1-I1^{i}	87.46(2)
Bi1-I1	3.1068(7)	I2-Bi1-I4	96.09(2)
Bi1-I2	3.1206(7)	I3-Bi1-I4	95.09(2)
Bi1-I2	3.2647(7)	I4-Bi1-I1^{i}	171.02(2)
Bi1-I1	3.3547(7)	I1-Bi1-I3	95.09(2)
X-M-X	**Bond angle, [°]**	**X-M-X**	**Bond angle, [°]**
I1-Bi1-I2^{ii}	88.75(2)	I1-Bi1-I4	89.61(2)
I2-Bi1-I1^{i}	86.01(2)	I2-Bi1-I3	90.37(2)
I3-Bi1-I1^{i}	93.62(2)	I2-Bi1-I2^{ii}	85.45(2)
I4-Bi1-I2^{ii}	88.30(2)	I3-Bi1-I2^{ii}	174.88(2)
		I1^{i}-Bi1-I2^{ii}	83.16(2)
M-X-M	**Bond angle, [°]**	**M-X-M**	**Bond angle, [°]**
Bi1-I1-Bi1^{i}	92.54(2)	Bi1-I2-Bi1^{ii}	94.55(2)
Symmetry codes: (i) 1-x,-y,1-z; (ii) 2-x,-y,1-z			
		HT-phase	
M-X	**Bond length, [Å]**	**X-M-X**	**Bond angle, [°]**
Bi1-I1 Bi1-I1^{i}	3.0783(4)×2	I2-Bi1-I1^{ii} I2^{i}-Bi1-I1iii	167.30(1)×2
Bi1-I2 Bi1-I2^{i}	2.9439(5)×2	I1-Bi1-I2^{i} I2-Bi1-I1^{i}	91.67(1)×2
Bi1-I1^{ii} Bi1-I1^{iii}	3.2944(5)×2	I2^{i}-Bi1-I1^{ii} I2-Bi1-I1^{iii}	89.41(1)×2
X-M-X	**Bond angle, [°]**		
I1-Bi1-I2 I1^{i}-Bi1-I2^{i}	86.63(1)×2	I1-Bi1-I1^{i}	177.31(2)
I1-Bi1-I1^{ii} I1^{i}-Bi1-I1^{iii}	88.03(1)×2	I1-Bi1-I1^{iii} I1^{i}-Bi1-I1^{ii}	94.05(1)×2
I2-Bi1-I2^{i}	102.25(2)	I1^{ii}-Bi1-I1^{iii}	79.49(1)
M-X-M	**Bond angle, [°]**		
Bi1-I1-Bi1^{ii}	91.98(1)		
Symmetry codes: (a) 1-x,y,3/2-z; (b) 1-x,1-y,1-z; (d) x,1-y,1/2+z			

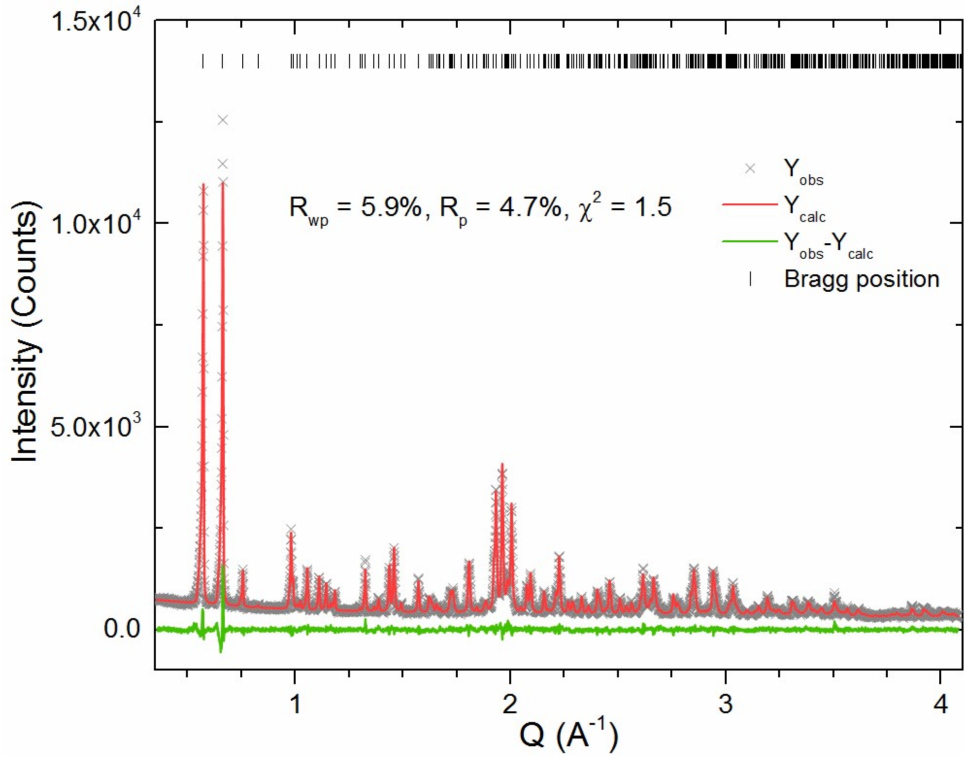

Figure S1. The final plot of Rietveld refinements on IEF-4 RT-phase ($BzImH[BiI_4]\cdot H_2O$).

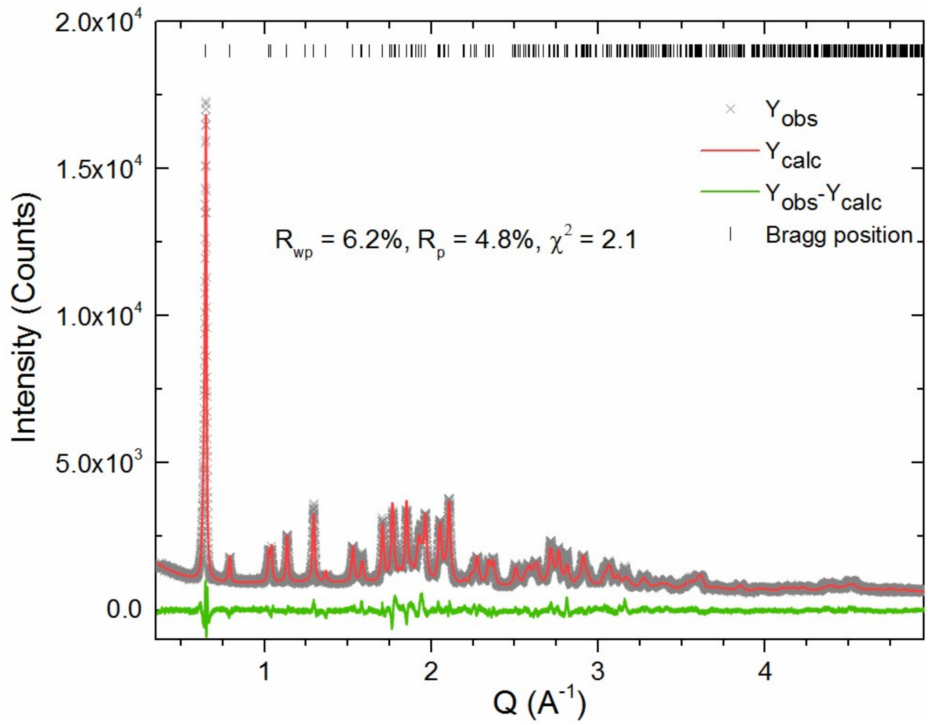

Figure S2. The final plot of Rietveld refinements on HT-phase ($BzImH[BiI_4]$) phase.

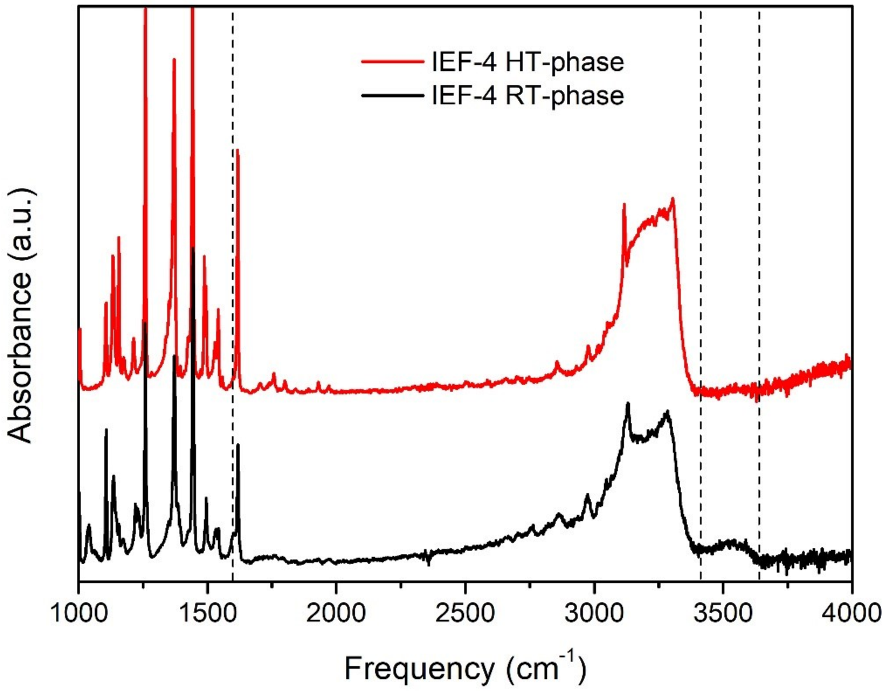

Figure S3. Comparison of FTIR spectra of IEF-4 RT- and HT-phases. The relevant parts are hold in dashed frames.

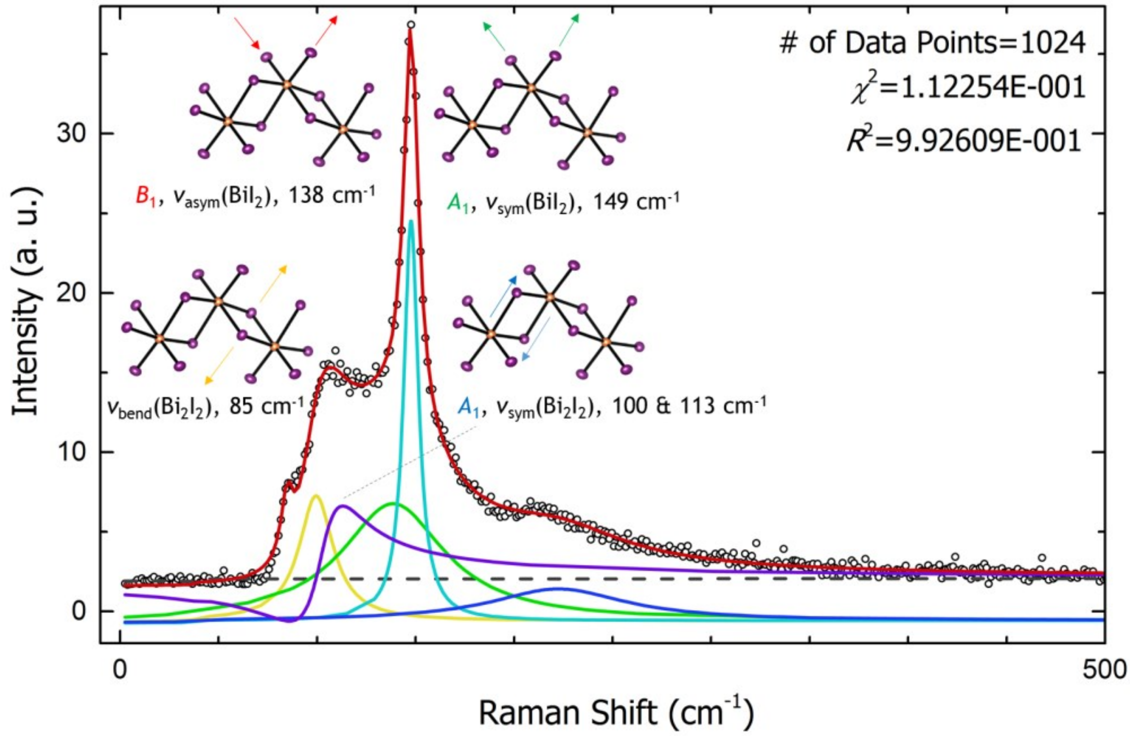

Figure S4. The individual band-decomposed Raman spectrum of IEF-4 RT-phase ($BzImH[BiI_4]\cdot H_2O$)

The peak deconvolution has been done using non-linear least squares algorithm. In the case of present study, Lorentzian of Voight (a convolution of Lorentzian and Gaussian line shapes) was found less stable than Breit-Wigner-Fano resonance lineshape**[S1]**:

$$I_F(\omega_s) = I_0 \frac{\left(1 + \frac{s}{q_F}\right)^2}{1 + s}, s = (\omega_s - \omega_G)/\Gamma$$

where ω_s, ω_G, $1/q_F$, Γ, and I_0 are the Raman shift, the spectral peak position, the asymmetric factor, the spectral width, and the maximum intensity of the spectra, respectively. It performed the best due to peak asymmetry, especially, in the case of $A_1/v_s(Bi_2I_2)$. This is likely due to the interaction of the optic phonon with a valence-band electronic continuum, as both the phonon and the electronic continuum Raman scatter the incident radiation.

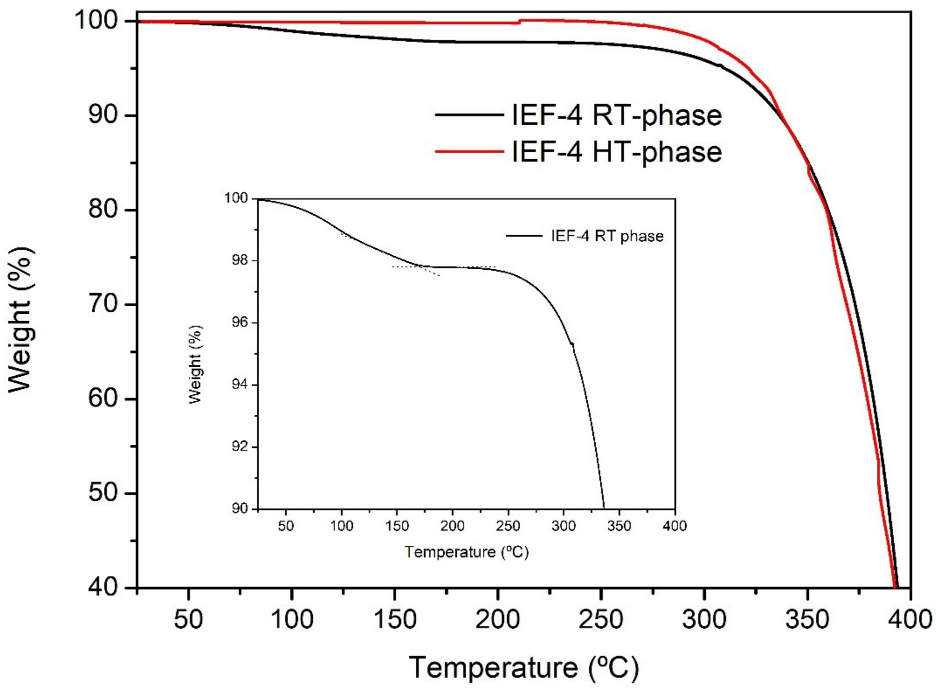

Figure S5. TGA plots of IEF-4 RT and HT phases. The inset corresponds to a zoom of the TGA of IEF-4 RT phase in order to better observe the departure of water molecules.

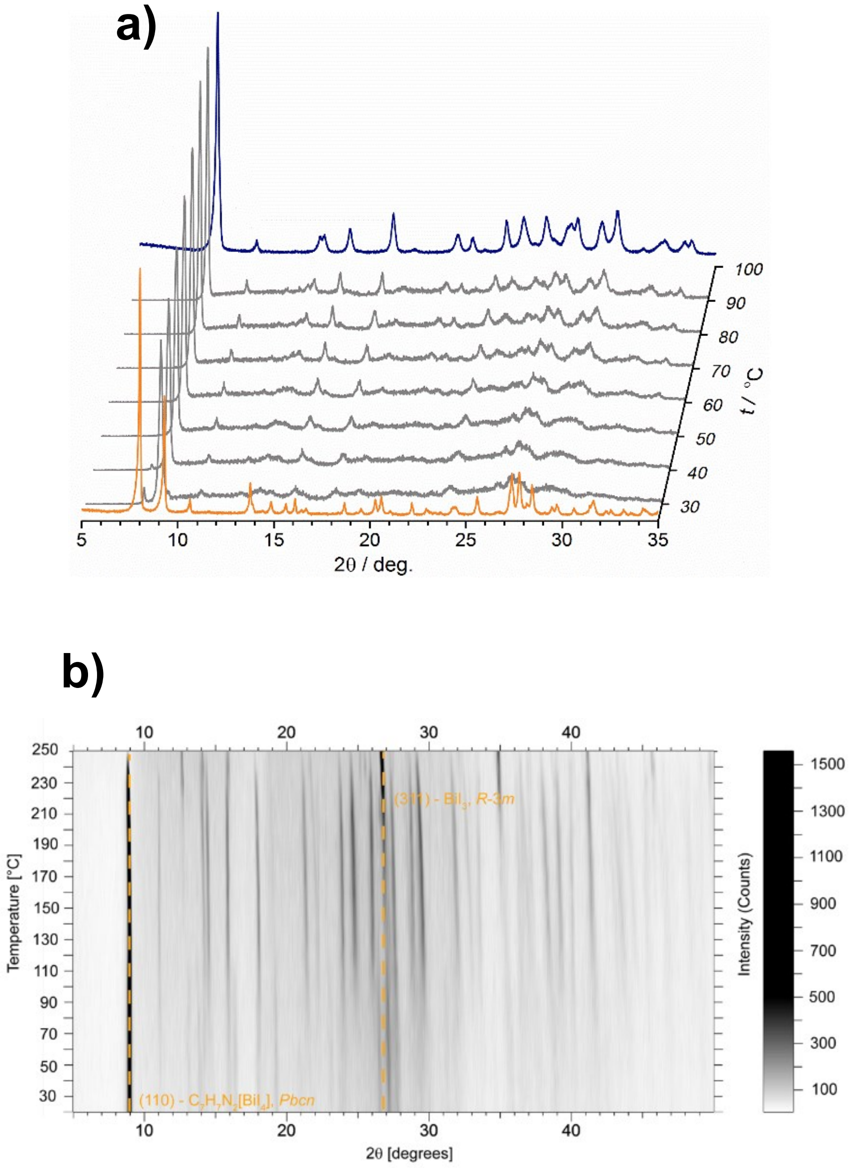

Figure S6. a) A comparative plot of IEF-4 RT-phase thermal evolution (from RT- to HT-phase) and b) T-PXRD patterns of the IEF-4 thermal decomposition.

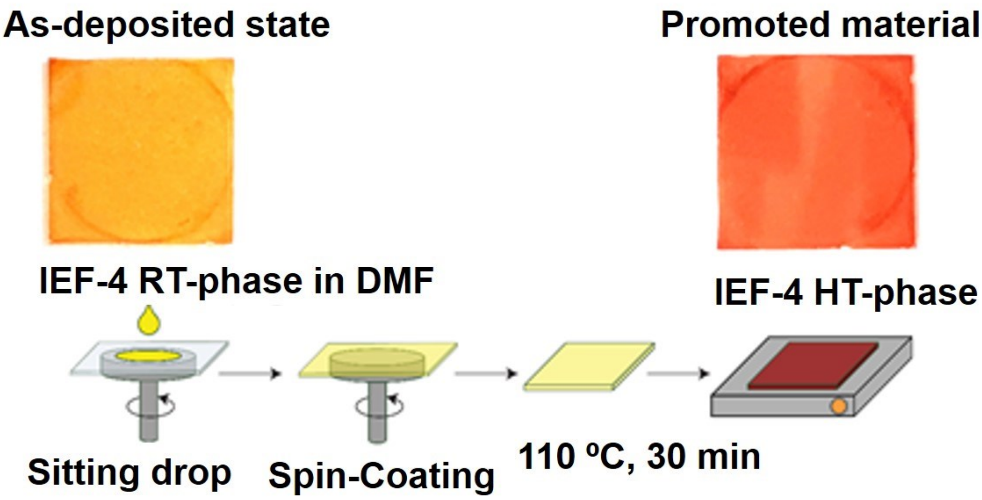

Figure S7. The scheme of applied deposition procedure. Note the change of coating shade moving from top left to top right corner of the picture

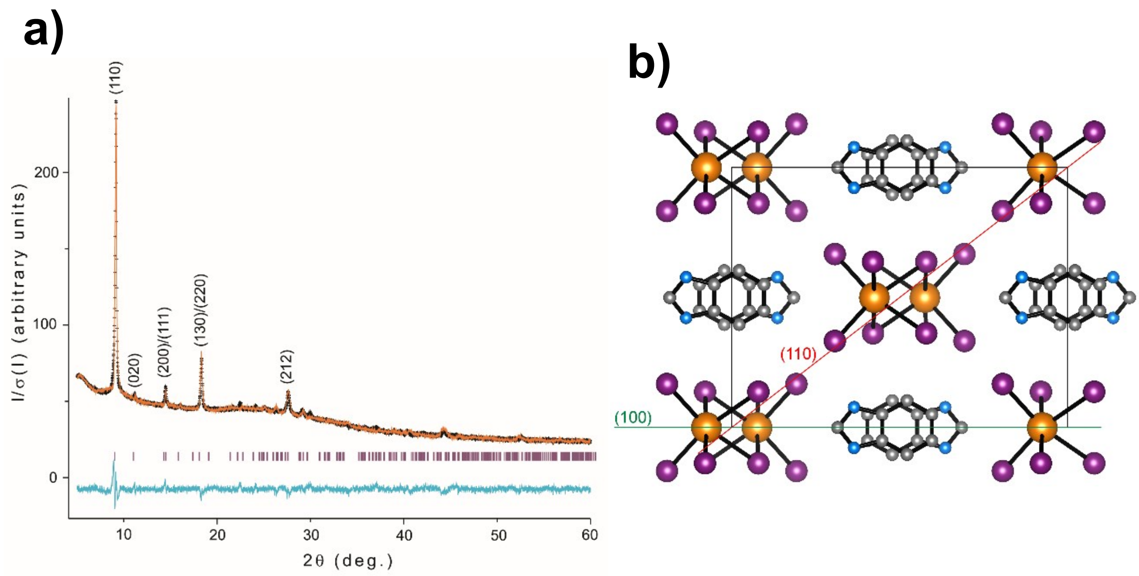

Figure S8. a) Rietveld refined pattern of deposited IEF-4 material acquired in 2θ-θ regime and b) Projection of HT-phase unit cell with drawn Miller planes corresponding to the texture.

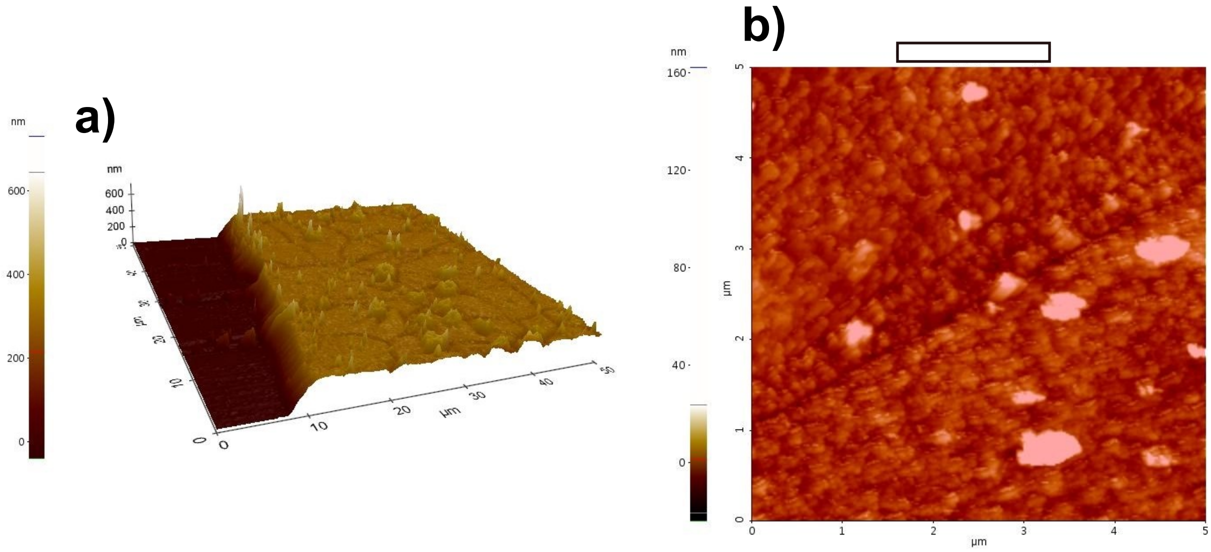

Figure S9. AFM images of IEF-4 thin film a) 3D image and b) 2D image

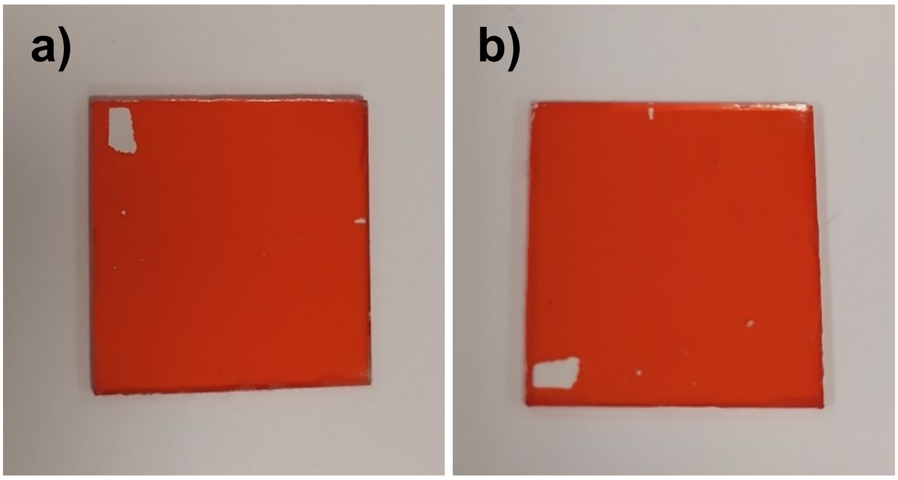

Figure S10. Photographs of IEF-4 thin film a) fresh film and b) after of humidity exposure for 8 days (RH = 53%)

REFERENCES:

(S1) Fano, U. Effects of Configuration Interaction on Intensities and Phase Shifts. *Phys*. *Rev*. **1961**, 124, 1866

(S2) Pyykkö, P. Strong Closed-Shell Interactions in Inorganic Chemistry. *Chem*. *Rev*., **1997**, *97*, 597–636.

(S3) Dennington, A.J.; Weller, M.T. Synthesis and Structure of Pseudo-three Dimensional Hybrid Iodobismuthate Semiconductors. *Dalton Trans*., **2016**, *45*, 17974–17979.